Discover Oncology

Analysis

Tumour-infiltrating immune cells as a novel prognostic model for bladder cancer

Can Liu[1] · Chaoyu Liao[1] · Bishao Sun[1] · Zhen Guo[2] · Sihao Chen[3,4] · Shixue Liu[2] · Xiaoyu Yuan[2] · Zeyu Huang[1] · Jingui Liu[1] · Min Deng[1] · Kui Wang[1] · Ruixin Wu[3,4] · Jiang Zhao[1] · Xingyou Dong[2]

Received: 16 October 2024 / Accepted: 2 April 2025
Published online: 11 May 2025

Abstract

Bladder cancer (BLCA) is the tenth most commonly diagnosed cancer and poses a significant challenge due to its complexity and associated high morbidity and mortality rates in the absence of optimal treatment. The tumor microenvironment (TME) is recognized as a critical factor in tumor initiation, progression and therapeutic response, and offers numerous potential targets for intervention. A comprehensive understanding of immune infiltration patterns in BLCA is essential for the development of effective prevention and treatment strategies. In this study, bioinformatics analysis was used to identify differentially expressed genes (DEGs) and tumor-infiltrating immune cells (TIICs) between BLCA tissues and adjacent normal tissues. Weighted gene co-expression network analysis (WGCNA) and protein–protein interaction (PPI) analysis were used to identify the top 10 hub genes with the most significant co-expression effects, and their potential relationship with patient prognosis was then predicted. The random survival forest (RSF) model was used to further identify six variables among the hub genes and establish a novel scoring system, defined as the tumor-infiltrating immune score (TIIS) to predict the prognosis of BLCA patients. In addition, the correlation analysis between TIIS and drug sensitivity was investigated using the Genomics of Drug Sensitivity in Cancer (GDSC) and Cancer Therapeutics Response Portal (CTRP) databases. Patients with high TIIS were found to have a poor prognosis but may be more sensitive to Cisplatin and certain novel agents. This study provided a systematic analysis of immune cell infiltration in BLCA and established TIIS to predict patient prognosis and the efficacy of specific drugs in the treatment of BLCA.

Keywords Bladder cancer · Single cell atlas · Immune cell infiltration · Drug sensitivity · Tumor-infiltrating immune score

Abbreviations

BLCA	Bladder cancer
TME	Tumor microenvironment
DEGs	Differentially expressed genes

Can Liu, Chaoyu Liao, Bishao Sun and Zhen Guo have contributed equally to this work.

Supplementary Information The online version contains supplementary material available at https://doi.org/10.1007/s12672-025-02292-x.

✉ Ruixin Wu, ruixinwu@hospital.cqmu.edu.cn; ✉ Jiang Zhao, urologyzhaoj@sohu.com; ✉ Xingyou Dong, dongxingyou@hotmail.com | [1]Department of Urology, The Second Affiliated Hospital, Army Military Medical University, Chongqing 400037, China. [2]Urology Department, Chongqing Shapingba Hospital, School of Medicine, Chongqing University, Chongqing 400030, China. [3]Department of Immunology, School of Basic Medical Sciences, Chongqing Medical University, Chongqing 400010, China. [4]Chongqing Key Laboratory of Tumor Immune Regulation and Immune Intervention, Chongqing 400010, China.

TIICs	Tumor-infiltrating immune cells
WGCNA	Weighted gene co-expression network analysis
PPI	Protein–protein interaction
RSF	Random survival forest
TIIS	Tumor-infiltrating immune score
CAFs	Cancer-associated fibroblasts
EMT	Epithelial-to-mesenchymal transition
scRNA-seq	Single-cell RNA sequencing
ssGSEA	Single-sample gene set enrichment analysis
OS	Overall survival
RFS	Relapse-free survival
OOB	Out-of-bag
VIMP	Variable importance
ROC curve	Receiver operating characteristic curve
K–M curve	Kaplan–Meier curve
TMB	Tumor mutation burden
MSI	Microsatellite instability
TAMs	Tumor-associated macrophages

1 Introduction

Cancer is a major cause of global mortality and a significant barrier to increasing human longevity. Bladder cancer (BLCA) is the tenth most commonly diagnosed cancer worldwide [1]. BLCA is a multifaceted disease associated with significant morbidity and mortality in the absence of appropriate treatment [2]. Surgery is considered the primary treatment modality for BLCA, although the risk of recurrence remains due to incomplete tumor removal [3]. The 2022 European Society of Urology guidelines recommend the use of cisplatin-based neoadjuvant chemotherapy for patients with T2-4a and cN0M0 BLCA to improve 5-year survival by 8%. However, the use of neoadjuvant chemotherapy is limited in clinical practice, with only 17.2% of patients receiving this treatment due to the associated toxicity of cisplatin [4]. In recent years, there has been rapid development in the field of immunotherapy, which offers advantages such as improved targeting, reduced side effects, and improved efficacy compared to conventional chemotherapy. Significant progress has been made in the use of immunotherapy for the treatment of BLCA [5]. However, recent studies have shown that immune checkpoint inhibitors are only effective against certain subtypes of BLCA, highlighting the challenge of resistance to immunotherapy in the treatment of this disease [6]. Despite significant advances in cancer biology and treatment, clinical outcomes for patients with BLCA remain less than ideal. The tumor microenvironment (TME) has been identified as a critical factor in tumor initiation, progression, and management, and represents numerous potential targets for therapeutic intervention. Consequently, elucidation of immune infiltration patterns in BLCA is essential for the prevention and treatment of this disease and represents a primary area of investigation in current research.

Tumor-infiltrating immune cells (TIICs) play a critical role in the TME and contribute to the complex immune landscape within tumors [7]. Most immune cells have dual anti-tumor and pro-tumor effects. Research indicated that the IgG1/IgA ratio produced by infiltrating B cells in BLCA was correlated with prolonged patient survival, improved response to anti-PD-L1 therapy, increased incidence of cytotoxic activities in infiltrating immune cells, and enhanced TCR signaling associated with IL-21-mediated signaling [8]. In addition to CD8+ T cells, CD4+ T cells have been identified to mediate antitumor cytotoxicity in BLCA [9]. Another study showed that BLCA cells downregulated MHC II molecules to create an immunosuppressive microenvironment, leading to M2 polarization and differentiation of monocytes within the tumor site. In addition, it was reported that the LAMP3+ dendritic cells subset had the potential to attract regulatory T cells, potentially contributing to the development of an immunosuppressive TME [10]. Compared to normal urothelial cells in vitro, NK cells showed increased release of the degranulation marker CD107a and secretion of interferon γ. NK cells exhibited increased cytotoxicity against bladder cell lines and organoids, while also secreting the cytokines CCL1, CCL2, and CCL20 to promote T cell recruitment [11]. In addition, cancer-associated fibroblasts (CAFs) facilitated the epithelial-to-mesenchymal transition (EMT) of BLCA cells via paracrine IL-6 signaling, thereby promoting the invasive phenotype of non-invasive BLCA cells [12]. Investigation of the influence of immune infiltration on drug sensitivity in BLCA is ongoing and requires systematic evaluation of the role of immune cells and identification of key immune cell-related genes.

The advancement and widespread adoption of high-throughput sequencing technology has enabled the application of bioinformatics analysis in the discovery of novel genes and biomarkers associated with various diseases, such as tumors [13, 14]. The use of data from the Gene Expression Omnibus (GEO) and The Cancer Genome Atlas (TCGA) databases for tumor heterogeneity analysis has become a well-established technology. Tumor heterogeneity is a critical factor influencing drug efficacy and disease recurrence [15]. BLCA serves as a prototypical tumor model that exhibits heterogeneity along multiple dimensions, including genomic and developmental cellular variability within cancer cell populations, as well as the diverse array of cell types and intricate interactions present within the TME.

Single-cell RNA sequencing (scRNA-seq) has the potential to explore the heterogeneity present in complex biological systems. By comprehensively analyzing transcriptomic variability within tumor entities and precisely delineating gene expression patterns in both the tumor and TME, more effective prognostic and therapeutic molecular targets may be identified. The study of diverse tumor characteristics may facilitate the development of effective molecularly targeted therapies, while the analysis of TIICs may offer valuable perspectives for overcoming immune suppression and restoring innate immune surveillance [16]. Recent advances in predictive personalized oncology research have been driven by the availability of comprehensive pharmacogenomic databases such as the Cancer Cell Line Encyclopedia (CCLE), Genomics of Cancer Drug Sensitivity (GDSC), and Cancer Treatment Response Portal v2 (CTRPv2). The integration of single cell expression profiles for drug response prediction offers the opportunity to identify novel therapeutic targets for clinical drug intervention [17].

This study involved the identification of differentially expressed genes (DEGs) and differential TIICs between BLCA tissues and adjacent normal tissues using the GSE13507 dataset. The top 10 hub genes with the strongest co-expression effects were screened using weighted gene co-expression network analysis (WGCNA) and protein–protein interaction (PPI) analysis, and external validation was performed in the TCGA-BLCA dataset, yielding consistent results. In addition, the expression patterns of these 10 hub genes were analyzed in the scRNA-seq GES169379 dataset. Furthermore, the relationship between these 10 hub genes and patient prognosis was predicted using the TCGA-BLCA dataset, revealing an association with favorable patient outcomes. To identify prognosis-related hub genes, a random survival forest (RSF) model was used to screen six variables (CD2, CSF1R, CCL5, IRF8, TYROBP, and HLA-DRA) and to create a scoring system defined as tumor-infiltrating immune score (TIIS). Furthermore, we investigated the correlation between TIIS and drug sensitivity using the GDSC and CTRP databases. Our analysis revealed patients with higher TIIS may be more sensitive to Cisplatin and certain novel agents like fluvastatin, staurosporine. This investigation not only comprehensively examined immune cell infiltration in BLCA, but also established TIIS to predict patient prognosis and effective drugs for BLCA treatment, providing new perspectives for the treatment of BLCA.

2 Materials and methods

2.1 Data collection and preparation

The expression profile of GSE13507 was implemented based on the GEO (https://www.ncbi.nlm.nih.gov/geo/), a public database containing comprehensive gene profile analysis and sequencing data. GSE13507 included 58 cases of bladder mucosa surrounding cancer, 1 case of multipotent progenitor cells, 9 cases of normal bladder mucosa, 165 cases of primary BLCA, and 23 cases of recurrent non-invasive tumors. Our analysis included 58 cases of paracancerous tissues and 9 cases of normal bladder mucosa, a total of 67 samples were used as normal controls, and 165 cases of primary BLCA were used as tumor samples [18, 19]. TCGA (https://portal.gdc.cancer.gov/) is a landmark cancer genomics database that mainly contains clinical data on various human cancers, such as genomic variation, mRNA expression, miRNA expression, methylation, and other data. Our study included a total of 400 patients with primary BLCA and 18 normal controls. The complete clinical information of these patients was obtained from the TCGA database. In addition, we also obtained pan-cancer genomic information. The immunotherapy dataset (IMvigor210) was downloaded using the R package "IMvigor210CoreBiologies" [20]. GSE48075 contained 142 samples and our study included its internal 73 samples with survival data [21, 22]. The scRNA-seq dataset GSE169379 was a single-cell dataset to study the survival prognosis of BLCA. Our analysis included all tumor cells involved in this dataset, a total of 25,209. Relevant cell annotation information was taken from the H5AD file provided by the author [23]. GSE13507 was sequenced on the GPL6102 platform (Illumina human-6 v2.0). The R package "IOBR" was used for data processing. After eliminating redundant data, probes corresponding to repeated genes were replaced with the average expression levels [24]. GSE169379 data was

processed using Seurat V5.01 software for cell quality control, expression homogenization, standardization, dimensionality reduction, and clustering [25].

2.2 Identification of DEGs

In this study, we used the "limma" package to discover the DEGs between BLCA tissues and normal tissues from the GSE13507 dataset. Based on normalized gene expression levels, adjusted $p < 0.05$ and $|\log2 \text{ fold change}| > 1$ were used as criteria for selecting significant DEGs [26].

2.3 Evaluation of the TIICs

The single-sample gene set enrichment analysis (ssGSEA) method is a recently proposed algorithm for calculating immune cell subpopulations using RNA samples from various tissue types, including solid tumors. It contains less noise and unknown mixtures than other methods, and the cell types are closely related. In this study, the ssGSEA method was used to calculate the absolute enrichment scores of 28 TIICs in 165 BLCA patients and 58 controls in the GSE13507 dataset, and used heat maps and box plots to display them [27].

2.4 Establishing WGCNA based on TIICs

WGCNA is a method that reconstructs free-scale gene co-expression networks and simultaneously identifies modules composed of highly correlated genes to evaluate the association between external clinical features and modules [28]. In this study, we applied R package "WGCNA" to analyze the GSE13507 microarray dataset containing 165 BLCA tissues. First, a weighted adjacency matrix was calculated to represent the connection strength of each pair of genes, and outliers were eliminated to ensure a co-expression network. The soft threshold power was set to 6 to obtain a scale-free topology network. Then, a hierarchical clustering dendrogram consisting of enriched branches was constructed, and each branch was assigned a color to reveal a module. Finally, module-trait association was used to analyze the association of modules with TIICs based on module membership and gene significance.

2.5 Construction of PPI network

PPIs were identified and predicted using the Interacting Gene/Protein Search Tool (STRING) database (https://string-db.org/) [29]. After establishing the PPIs, Cytoscape was used to visualize the PPIs and determine the top 10 hub genes of the network based on the degree value [30].

2.6 Functional enrichment

Metascape (http://metascape.org) is a friendly, reliable tool for functional enrichment analysis. The minimum number of overlaps and the minimum number of enrichment were both set to 3, and the P-value cutoff was set to 0.05. Next, we performed enrichment analysis of hub genes on this site [31].

2.7 GEPIA analysis

Gene Expression Profiling Interactive Analysis (GEPIA, http://gepia2.cancer-pku.cn, version 2) is an open-access online tool for interactive exploration of TCGA and Genotype-Tissue Expression Project (GTEx) RNA sequencing data from 9736 tumor and 8587 normal samples [32]. In this study, GEPIA2 was used to calculate the prognostic index for each selected gene. The minimum P cutoff value was used as the dividing line for both low and high expression groups, and the Kaplan–Meier method was used to evaluate the overall survival (OS) and relapse-free survival (RFS) of patients. The log-rank test (Mantel-Cox test) was used for hypothesis testing, and a p value of less than 0.05 was considered statistically significant.

2.8 scRNA-seq analysis

Single-cell RNA sequencing provides higher resolution than bulk RNA sequencing and can unveil heterogeneity between cells. In this study, we focused on the expression of hub genes on the BLCA cell map and visualized the corresponding results using R package "scpubr".

2.9 Construction of TIIS model

RSF is an integrative algorithm that first uses the bootstrap sampling method to randomly select N samples from the training queue to generate N survival trees, and then randomly selects a subset of covariates at each node of the tree as candidate variables for splitting [33]. Thus, each tree consists of a classification or splitting node variable, and the tree nodes are split according to the maximum survival rate difference between the child nodes. The maximum survival rate difference can be calculated by four methods, namely log-rank, event preservation, log-rank scores and randomness. In this study, the log-rank method was used. For each bootstrap sample, on average, approximately 37% of the samples in the training cohort were not extracted, and these samples were called out-of-bag (OOB) samples. We calculated the OOB error rate for the OOB samples. The OOB error rate and the prediction error rate on the validation set were used to evaluate the performance of the model. The lower the error rate, the better the performance of the model. In this study, the error rate of the bags in the training queue under different parameter combinations was calculated by grid search to determine the best parameter combination of the model [34]. Finally, the parameter combination with the lowest overall RSF error rate was determined. An RSF model was constructed using optimal parameters, and variables were filtered based on variable importance (VIMP). The importance score was an evaluation index used to measure the predictive ability of the predictor variables. The higher the VIMP value, the stronger the predictive ability. A positive VIMP value indicated that the variable was predictive. If VIMP was 0 or negative, the variable was not a meaningful predictor. We selected the 6 most important variables and established a scoring system, defined as TIIS. C-index and calibration curves were used to evaluate model performance.

2.10 Tumor immune analysis of TIIS

IOBR is an R package focused on deciphering the TME. In this study, its 8 built-in immune algorithms were used to decode the TME on 400 BLCA samples from the TCGA cohort, including CIBERSORT, ESTIMATE, quanTIseq, TIMER, IPS, MCPCounter, xCell, and EPIC [35–41].

2.11 Drug sensitivity analysis of TIIS

We used the R package "oncoPredict" [42] to predict drug response for each patient in the TCGA cohort based on the Genomics of Drug Sensitivity in Cancer (GDSC) (https://www.cancerrxgene.org/) and Cancer Treatment Response Portal (CTRP) databases.

2.12 Pan-cancer analysis

TCGAplot is an R package for comprehensive pan-cancer analysis and visualization of TCGA multi-omics data [43]. In this study, the R package was used to perform pan-cancer correlation analysis on 6 model variables, including pan-cancer single-factor COX analysis, pan-cancer TMB analysis, pan-cancer MSI analysis, differential expression analysis of paired samples. Furthermore, correlation analyses between the 6 model variables and immune cells, immune checkpoints and receptors were performed.

2.13 Statistical analysis

All statistical analyses were performed with R software (version 4.3.2). Kaplan–Meier analysis and log-rank test were used to assess survival and to compare differences in survival between cohorts and risk groups. Two-sided $p < 0.05$ was considered statistically significant.

3 Results

3.1 Identification of DEGs and differential TIICs

We obtained a total of 165 BLCA samples and 67 adjacent normal samples from the GSE13507 database and the detailed description of our workflow was depicted in Fig. 1. Differential analysis was performed using the "limma" package. The result of DEGs shown as a volcano plot (Fig. 1A) indicated the presence of 341 downregulated genes and 56 upregulated genes in tumor tissues. Furthermore, for a more comprehensive analysis of the differences in TIICs between the two sample groups, we used the GSVA package and the ssGSEA function to perform a quantitative assessment on 28 immune cell types that have been previously documented. The results showed a significant downregulation of activated B cells, activated dendritic cells, central memory CD8+ CD4+ T cells, monocytes and NK cells in tumor tissues compared to normal tissues (Fig. 1B and C). This suggested that TIICs played an immunosuppressive role within the TME.

3.2 Identification of key genes for TIICs

In biology, gene functions are often manifested by co-expression networks. To evaluate the relationship between the DEGs and TIICs, we used weighted gene WGCNA to thoroughly investigate the gene co-expression patterns of 165 tumor samples within the GSE13507 dataset. By applying a module similarity threshold of 75%, we merged 13 co-expressed modules (Fig. 2A). Further investigation of the relationship between modules and TIICs scores revealed a significant correlation between the METan module and the majority of TIICs scores (Fig. 2B). In the METan module, a total of 323 genes were screened and subjected to intersection analysis with the DEG set consisting of 397 genes, resulting in the identification of 35 intersection genes (Fig. 2C). Through a comprehensive PPI analysis of the 35 genes, our study identified the top 10 genes with the most pronounced co-expression effects, namely HLA-DPA1, CCL5, CD2, PLEK, HLA-DRA, CSF1R, CD48, IRF8, TYROBP and ITGB2, which were considered as hub genes in TIICs of BLCA (Fig. 2D).

3.3 Analysis of gene expression patterns and functional enrichment of the hub genes

To investigate the expression patterns of the 10 core genes in tumors and normal tissues, we first used the GSE13507 dataset for validation (Fig. 3A), followed by the inclusion of 400 BLCA samples and 19 adjacent normal samples from the TCGA database for additional analysis (Fig. 3B). With the exception of CCL5 ($p = 0.084$), which did not show significant differences in the TCGA-BLCA dataset, the remaining core genes showed consistent trends in both datasets. In addition, correlation analysis was performed on the 10 core genes within the GSE13507 (Fig. 3C) and TCGA-BLCA (Fig. 3D) datasets. The results confirmed the presence of positive correlation in the expression patterns of these core genes, strongly suggesting the significant contribution of these core genes to BLCA. To improve our knowledge of their biological functions, we performed functional enrichment analysis and cellular expression pattern analysis of the core genes using the Metascape website. The results of enrichment analysis (Fig. 3E and Supplementary Fig. 1) elucidated the primary biological processes associated with these genes, such as cell activation, cytokine signaling, and immune system cytokine pathways. Cell expression pattern analysis (Fig. 3F) highlighted the upregulated expression of these genes in various immune cell types, including NK cells, macrophages, myeloid cells, dendritic cells, and antigen-presenting cells.

3.4 scRNA-seq data reveals variation in hub genes expression in BLCA

To further validate the expression patterns of hub genes in bladder tumor cells, high-resolution single-cell data was used to analyze the ten identified hub genes. The BLCA GSE169379 scRNA-seq dataset was used for this analysis.

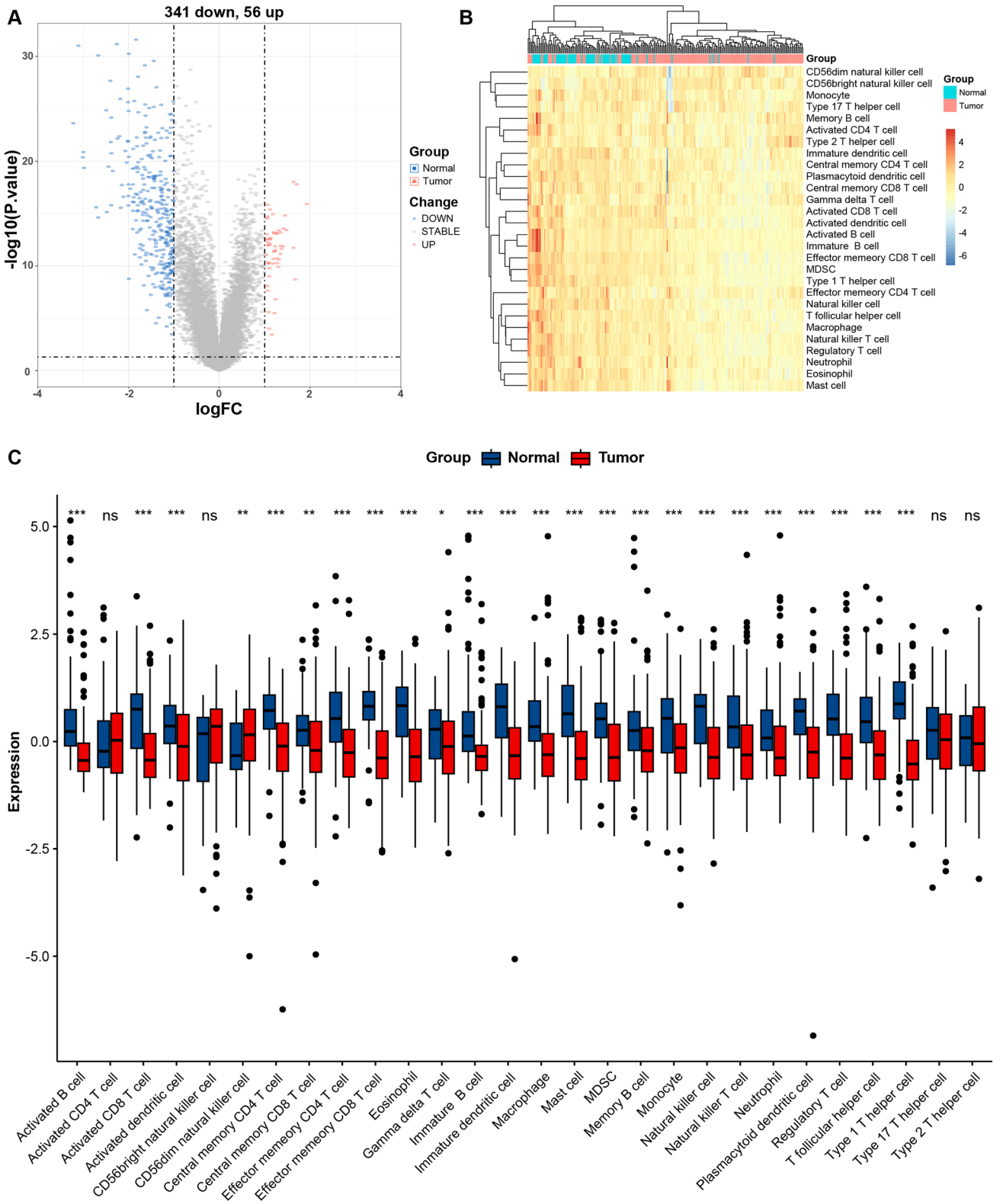

Fig. 1 Identification of differential genes and TIICs between tumor and normal samples. **A** Volcano plot of DEGs between tumor and normal samples from the GSE13507 database. **B** Heatmap of TIICs of samples from GSE13507 database. **C** Box plot of the levels of TIICs

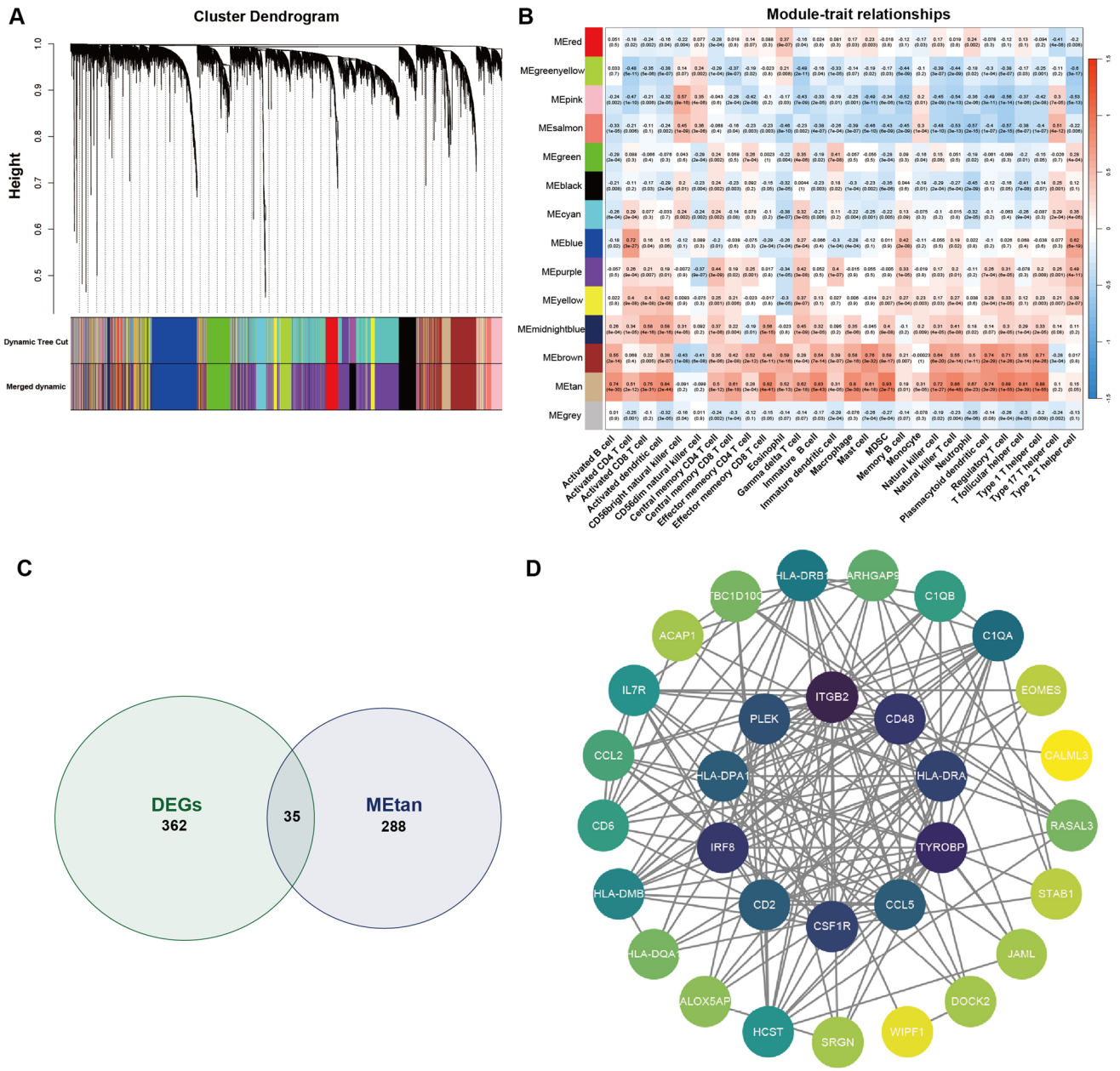

Fig. 2 Identification of the TIICs-related hub genes. **A** Cluster dendrogram of genes assigned to modules and merged modules. **B** Heatmap illustrating the correlation between immune traits of the GSE13507 cohort and module genes. **C** The Venn plot of DEGs and genes in the MEtan module. **D** Network plot showing the hub genes of the intersected genes

Initially, a resolution of 0.8 was chosen for dimensionality reduction of the dataset, resulting in the identification of five distinct cell groups: Endothelial, Epithelial, Fibroblast, Lymphocyte and Myeloid (Fig. 4A). Hub genes were indicated by the weighted kernel density, with HLA-DPA1 and HLA-DRA being predominantly expressed in epithelial cells, whereas CCL5, CD2 and CD48 were predominantly expressed in lymphocytes. At the same time, PLEK, CSF1R, IRF8, TYROBP, and ITGB2 were predominantly expressed in lymphocytes and myeloid cells (Fig. 4B–K). To provide additional evidence, violin plots were used to assess the distribution status and probability density of the genes (Fig. 4L), which yielded consistent results. Examining the results across different data sets clearly illustrated the distinct expression profiles of hub genes within different subpopulations of BLCA cells.

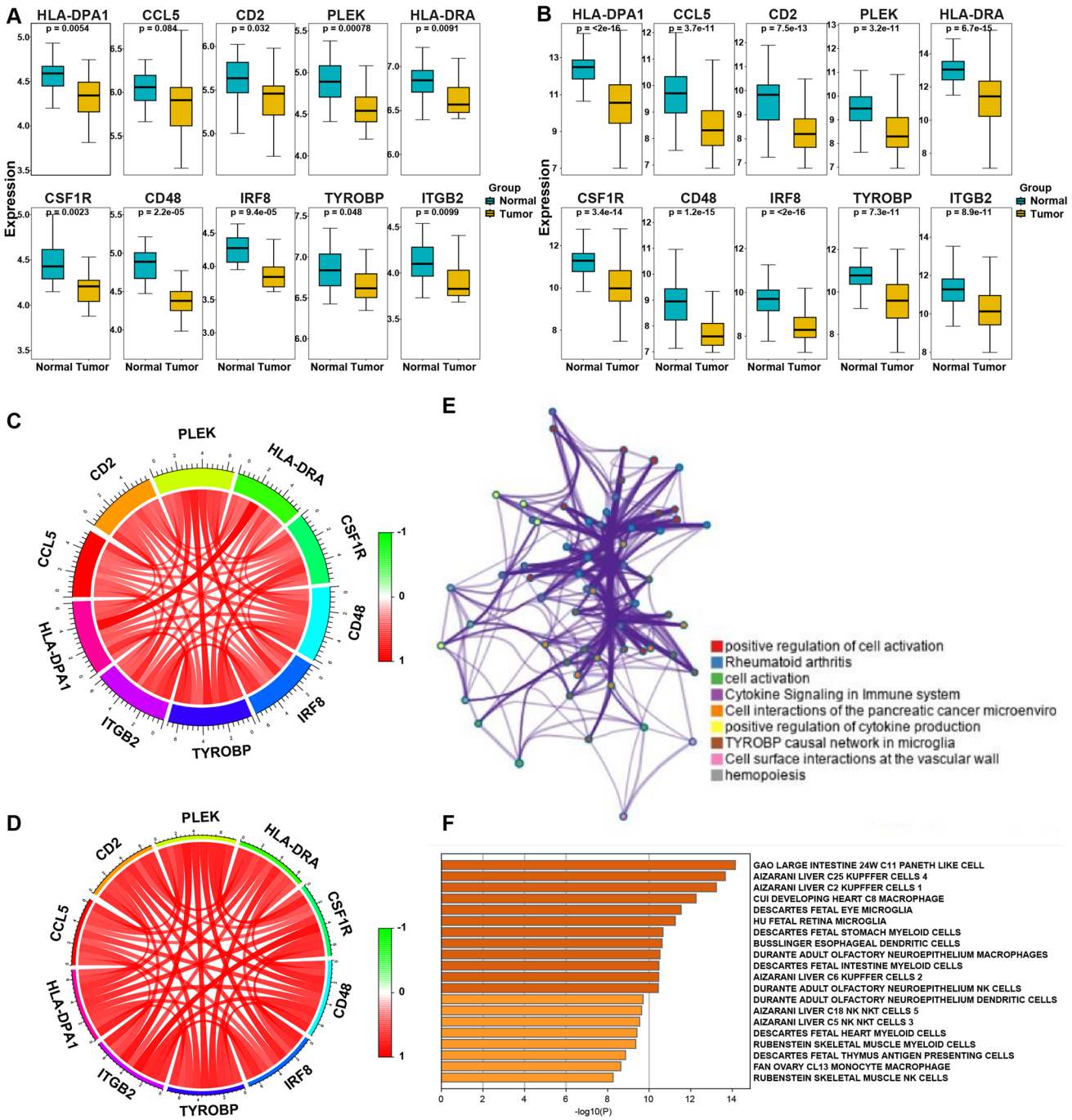

Fig. 3 Exploring the biological functions of TIICs-related hub genes. **A** Box plots of hub gene levels in tumor and normal samples from the GSE13507 dataset. **B** Box plots of hub gene levels in tumor and normal samples from the TCGA BLCA cohort. **C** Coexpression patterns of hub genes in the GSE13507 dataset. **D** Coexpression patterns of the hub genes in the TCGA BLCA cohort. **E** Network diagram showing the functional enrichment of the hub genes. **F** Bar graph showing the cell expression patterns of the hub genes

3.5 Analysis of hub genes for prognosis

To investigate the correlation between the identified hub genes and patient prognosis, we performed survival analysis using GEPIA2 on the TCGA-BLCA dataset. The results of the analysis showed that patients with elevated expression

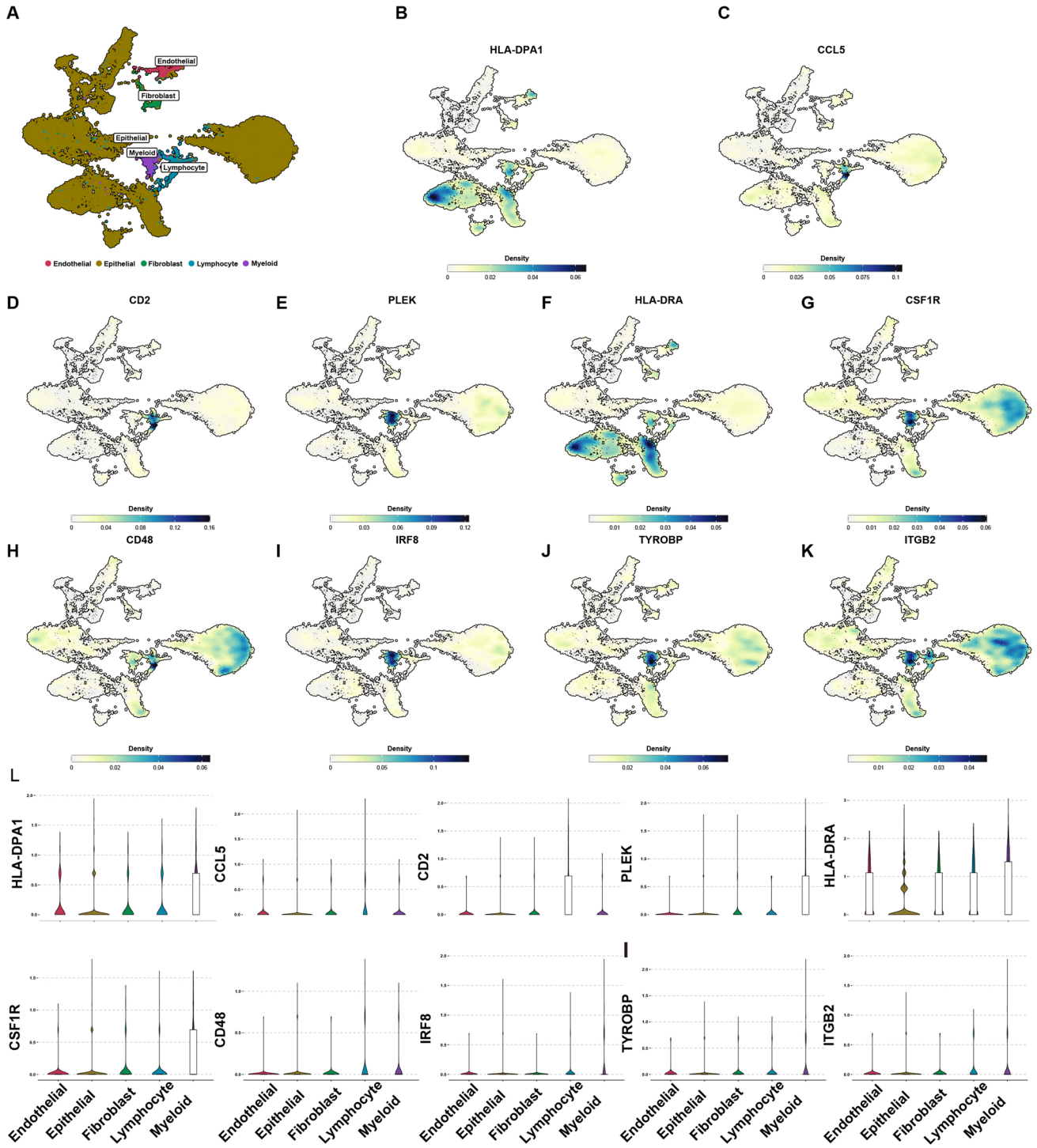

Fig. 4 Exploring the distribution of hub genes at single cell resolution. **A** Cluster annotation of the GSE169379 scRNA-seq dataset. **B**–**K** Feature plot showing the distribution of hub genes. **L** Violin plot showing the expression levels of hub genes in 5 cell types

levels of HLA-DRA, CD2, and CCL5 had a statistically significant improvement in survival (HR < 1 & p < 0.05) (Fig. 5). The Kaplan–Meier (K–M) curves showed that all hub genes significantly increased expression levels, resulting in prolonged RFS in patients (Supplementary Fig. 2). Overall, the ten identified hub genes were shown to significantly influence the prognosis of patients with BLCA.

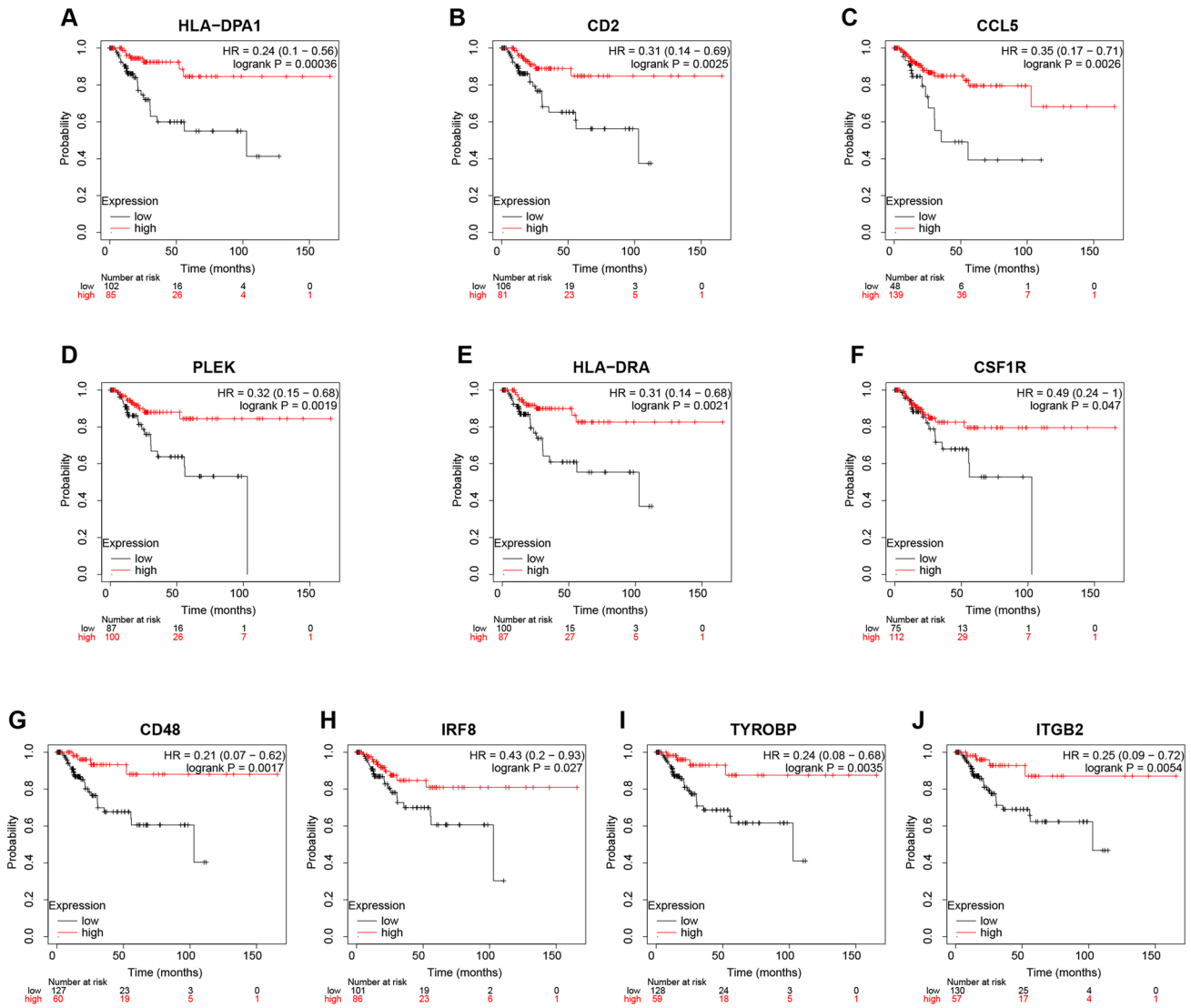

Fig. 5 Investigation of the significance of hub genes in predicting prognosis. **A**–**J** K–M curves showing the significance of hub genes in predicting OS

3.6 Establishing TIIS based on hub genes

To further screen for hub genes associated with prognosis, we constructed an RSF model based on the TCGA-BLCA dataset. The VIMP method was used to prioritize variable importance, which was then integrated with the minimum depth method to determine the number of nodes on the most direct path from the root node to the nearest leaf node for the purpose of filtering model variables. The reduction in the prediction error rate and the improvement in the overall stability of the prediction model were achieved with an increased number of trees (Fig. 6A and B). We screened out 6 variables, CD2, CSF1R, CCL5, IRF8, TYROBP and HLA-DRA (Fig. 6C and D), and developed TIIS based on them. To further investigate the prognostic implications of TIIS, the TCGA-BLCA dataset was divided into a high-TIIS group and a low-TIIS group. The prognosis of patients in the high-TIIS group was found to be significantly worse compared to those in the low-TIIS group. (Fig. 6E). The receiver operating characteristic (ROC) curve showed strong predictive performance (with an AUC > 0.8) at different time points including 1 year, 3 years and 5 years (Fig. 6F). Prognostic forest plot analysis showed that both N stage and TIIS were identified as independent risk factors for patient prognosis ($p < 0.05$) (Fig. 6G). The decision curve analysis (DCA) showed that TIIS provided superior clinical

Fig. 6 Construction of TIIS and efficiency validation. **A**–**D** RSF algorithm helps to reduce the number of model genes and we finally selected 6 genes as model variables. TIIS was established. **E** K–M curves for OS in the high-TIIS group and the low-TIIS group in the TCGA BLCA cohort, IMvigor210 and GSE48075 datasets. **F** Time-dependent ROC curves for 1-year, 3-year, and 5-year OS were generated for the 3 datasets. **G** Forests plots of multiple factors. **H** DCA curves of multiple factors

benefit when the risk exceeded 25% (Fig. 6H). The model was subsequently validated in two additional datasets, IMvigor210 and GSE48075, demonstrating consistent results with the original training set.

Furthermore, we conducted an analysis to compare the TIIS across the five molecular subtypes described by Robertson et al. [44], which serve as a key reference for molecular subtyping in BLCA histotype (Supplementary Fig. 3). Notably, we observed that the neuronal subtype, characterized by poor survival outcomes, exhibited the highest TIIS levels. Conversely, the luminal papillary subtype, predominantly node-negative and associated with younger patients and better survival, demonstrated the lowest TIIS levels. These findings reinforced the prognostic value of TIIS, highlighting its correlation with poor outcomes. Furthermore, the elevated TIIS in the neuronal subtype suggested its potential utility in identifying neuroendocrine phenotypes within BLCA.

3.7 Analysis of TIIS with immune cells and sensitivity to drugs

To further investigate the characteristics of the six variables involved in TIIS, we used eight different methods including Cibersort, EPIC, estimate and IPS for analysis. We found that TIIS was mainly associated with CD4+ T cells, CD8+ T cells and other T cell subsets. Fibroblasts showed a negative correlation with TIIS, whereas macrophages, endothelial cells, monocytes showed a positive correlation with TIIS (Fig. 7A). Using the TCGA cohort, our ssGSEA analysis revealed some intriguing findings. While we had expected significant differences in immune dysfunction, the high-TIIS and low-TIIS groups did not show substantial differences in CD8+ T cell dysfunction, immune regulation, or inflammatory responses (Supplementary Fig. 4A–C). This finding suggested that, although high TIIS was negatively correlated with T cell abundance, it might not have directly indicated dysfunction or suppression of specific immune responses.

Interestingly, however, high-TIIS tumors exhibited distinct enrichment in pathways related to angiogenesis, EMT, and glycolysis (Supplementary Fig. 4D–F). These results suggested that the primary immunosuppressive characteristics of high-TIIS tumors might have been mediated by non-immune mechanisms, such as increased angiogenic activity, metabolic reprogramming, and stromal remodeling, rather than a direct suppression of T cell activity.

Using the GDSC and CTRP databases, we performed drug sensitivity analyses to interpret the clinical applicability of TIIS. The imputed sensitivity scores of commonly used chemotherapy drugs, including Cisplatin, Vinblastine, and Gemcitabine, were found to be negatively correlated with TIIS (Fig. 7B). This indicates that patients with high TIIS are more likely to benefit from these drugs. Violin plots further revealed significant differences in drug responses between high-TIIS and low-TIIS groups. Notably, high-TIIS patients showed greater sensitivity to Cisplatin, while Methotrexate appeared to be more beneficial for low-TIIS patients (Fig. 7C, Supplementary Fig. 5A–C). Next, we identified the most sensitive drugs for the high-TIIS group using the GDSC and CTRP databases (Supplementary Fig. 5D–I). Compounds such as RO-3306 (a cell cycle inhibitor), NU7441 (a DNA repair inhibitor), AZD8055 (an mTOR inhibitor), DBeQ (a proteasome inhibitor), Staurosporine (a protein kinase inhibitor), and Fluvastatin (a lipid-lowering drug) exhibited better drug responses in the high TIIS group. Among these, Fluvastatin is a clinically approved cholesterol-lowering drug, whereas the others are primarily research compounds targeting cancer-related pathways. These findings highlight potential therapeutic opportunities, especially for BLCA patients with high TIIS.

To assess the relationship between TIIS and immunotherapy responses, we analyzed data from the IMvigor210 cohort, which includes BLCA patients treated with atezolizumab, a PD-L1/PD-1 immune checkpoint inhibitor. Our results showed that patients with SD/PD exhibited significantly higher TIIS levels compared to patients with PR/CR (Fig. 7D). This finding suggests that higher TIIS is associated with poorer response to atezolizumab, further supporting the prognostic value of TIIS in predicting immunotherapy outcomes.

4 Discussion

In this study, BLCA samples from the GSE13507 dataset were stratified into 165 tumor samples and 67 para-cancer samples, resulting in the identification of 397 DEGs. In addition, differential infiltration patterns of 28 immune cell types were observed and 323 genes were identified within the MEtan module. The DEGs were then integrated with

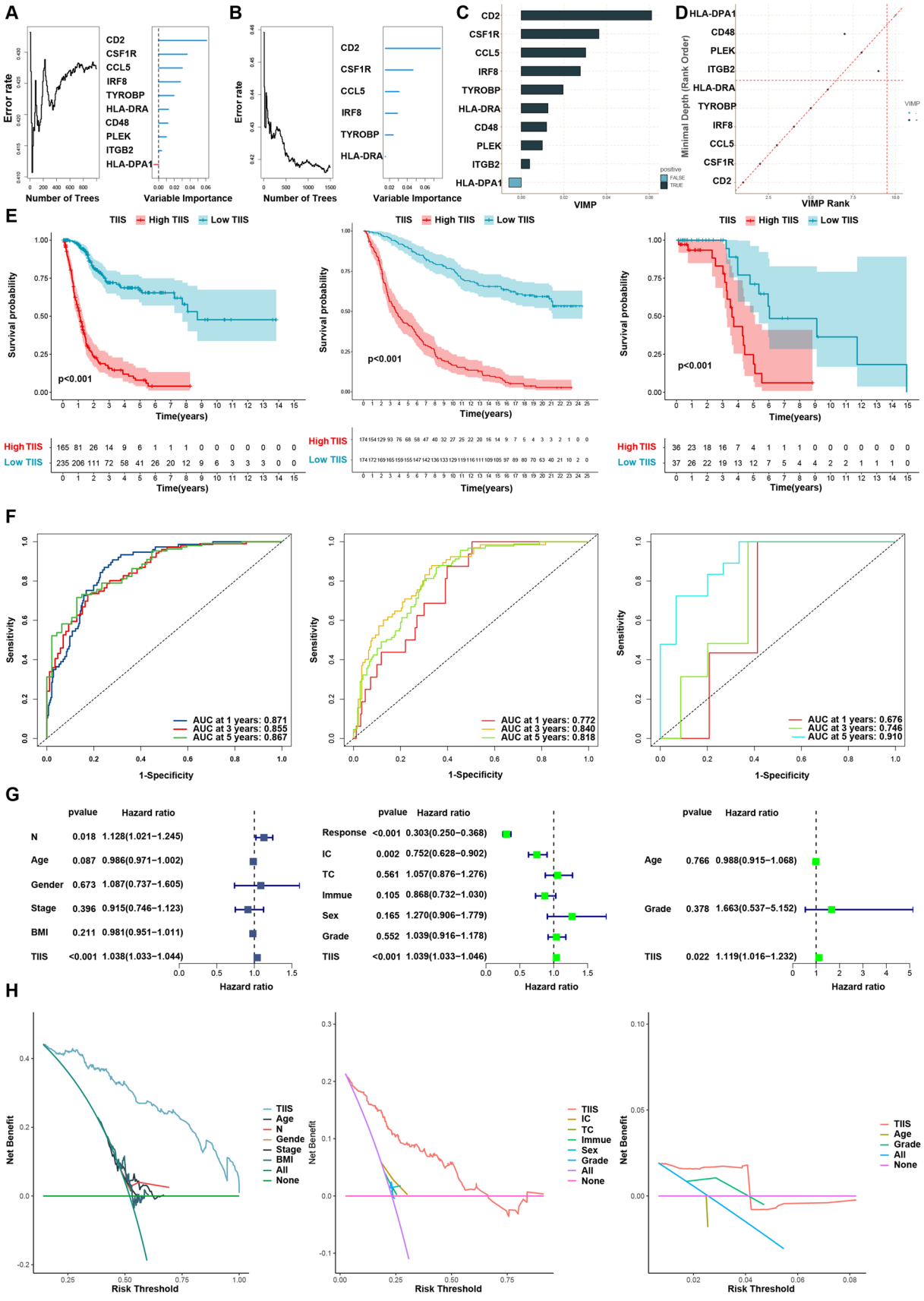
A
Error rate
Number of Trees
Variable Importance
CD2
CSF1R
CCL5
IRF8
TYROBP
HLA-DRA
CD48
PLEK
ITGB2
HLA-DPA1
B
Error rate
Number of Trees
Variable Importance
CD2
CSF1R
CCL5
IRF8
TYROBP
HLA-DRA
C
CD2
CSF1R
CCL5
IRF8
TYROBP
HLA-DRA
CD48
PLEK
ITGB2
HLA-DPA1
positive
FALSE
TRUE
VIMP
D
HLA-DPA1
CD48
PLEK
ITGB2
HLA-DRA
TYROBP
IRF8
CCL5
CSF1R
CD2
Minimal Depth (Rank Order)
VIMP Rank
VIMP
E
TIIS
High TIIS
Low TIIS
Survival probability
p<0.001
Time(years)
High TIIS 165 81 26 14 9 6 1 1 1 0 0 0 0 0 0 0
Low TIIS 235 206 111 72 58 41 26 20 12 9 6 3 3 3 0 0
High TIIS 174 154 129 93 76 68 58 47 40 32 27 25 22 20 16 14 9 7 5 4 3 3 2 1 0 0
Low TIIS 174 172 169 165 159 155 147 142 136 133 129 119 116 111 109 105 97 89 80 70 63 40 21 10 2 0
High TIIS 36 23 18 16 7 4 1 1 1 0 0 0 0 0 0 0
Low TIIS 37 26 22 19 13 12 7 5 4 4 2 2 1 1 1 0
F
Sensitivity
1-Specificity
AUC at 1 years: 0.871
AUC at 3 years: 0.855
AUC at 5 years: 0.867
AUC at 1 years: 0.772
AUC at 3 years: 0.840
AUC at 5 years: 0.818
AUC at 1 years: 0.676
AUC at 3 years: 0.746
AUC at 5 years: 0.910
G
pvalue
Hazard ratio
N 0.018 1.128(1.021−1.245)
Age 0.087 0.986(0.971−1.002)
Gender 0.673 1.087(0.737−1.605)
Stage 0.396 0.915(0.746−1.123)
BMI 0.211 0.981(0.951−1.011)
TIIS <0.001 1.038(1.033−1.044)
Response <0.001 0.303(0.250−0.368)
IC 0.002 0.752(0.628−0.902)
TC 0.561 1.057(0.876−1.276)
Immue 0.105 0.868(0.732−1.030)
Sex 0.165 1.270(0.906−1.779)
Grade 0.552 1.039(0.916−1.178)
TIIS <0.001 1.039(1.033−1.046)
Age 0.766 0.988(0.915−1.068)
Grade 0.378 1.663(0.537−5.152)
TIIS 0.022 1.119(1.016−1.232)
Hazard ratio
H
Net Benefit
Risk Threshold
TIIS
Age
N
Gende
Stage
BMI
All
None
TIIS
IC
TC
Immue
Sex
Grade
All
None
TIIS
Age
Grade
All
None

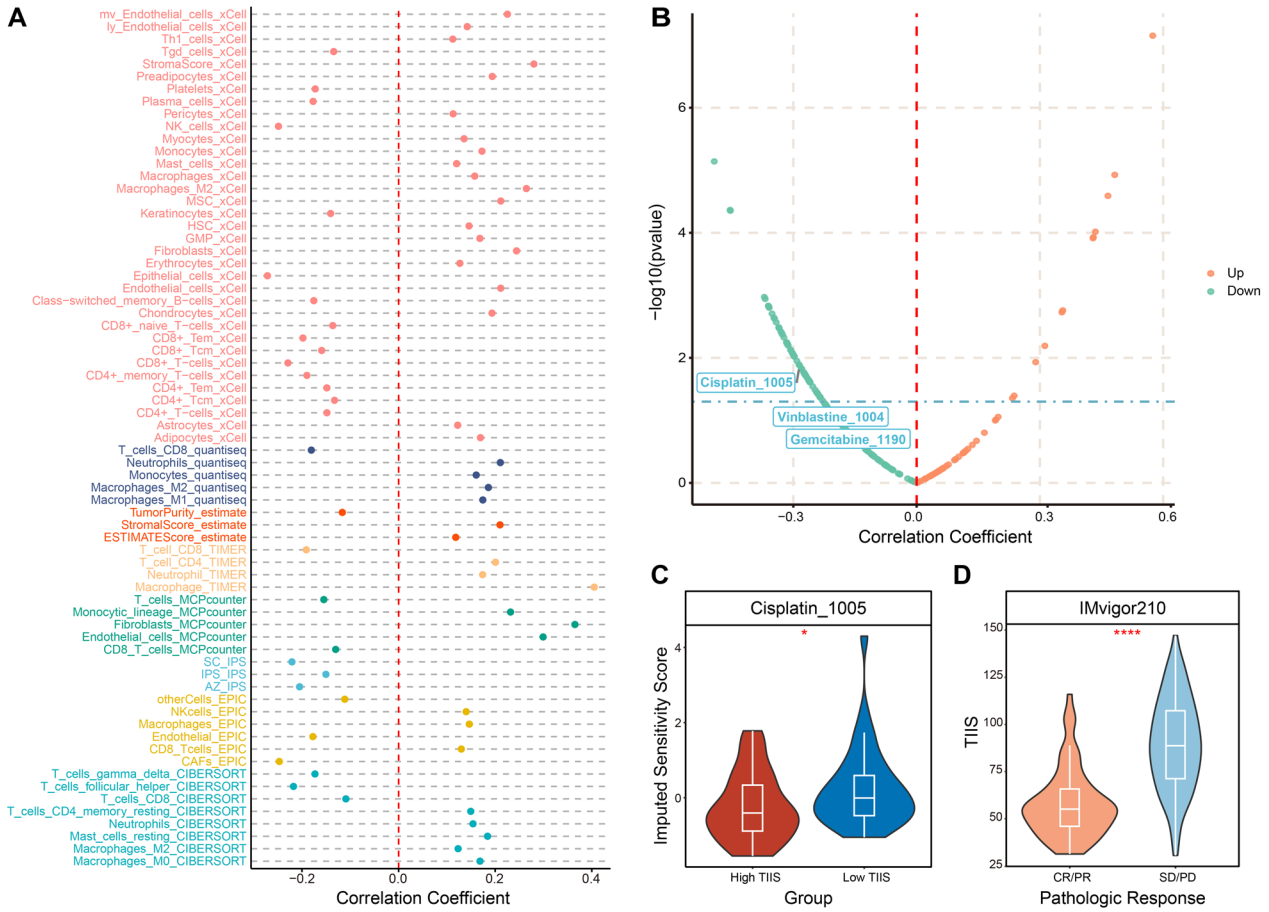

Fig. 7 Investigation of the correlations of TIIS with immune cells and drug sensitivity. **A** Dot plot showing the correlation levels of TIIS and various TIICs using different algorithms. **B** The correlation levels of TIIS and imputed sensitivity scores of different drugs using the GDSC database. **C** Violin plot of imputed sensitivity score of Cisplatin for the high-TIIS group and low-TIIS group. **D** TIIS of patients with different pathologic responses in the IMvigor210 cohort

the module genes which were most associated with TIICs. Subsequently, the intersection gene underwent PPI analysis and identified 10 hub genes. External validation was then performed using the TCGA-BLCA dataset, which yielded consistent results. In addition, the expression patterns of 10 hub genes were analyzed in the scRNA-seq GES169379 dataset, revealing that HLA-DPA1 and HLA-DRA were predominantly expressed in epithelial cells, while CCL5, CD2 and CD48 were predominantly expressed in lymphocytes. In addition, PLEK, CSF1R, IRF8, TYROBP, and ITGB2 were predominantly expressed in myeloid cells. These findings suggested that the 10 hub genes played a critical role in improving the prognosis of patients with BLCA. In addition, the RSF model was used to identify six variables (CD2, CSF1R, CCL5, IRF8, TYROBP, and HLA-DRA) and establish a novel scoring system defined as TIIS for further analysis of prognosis and clinical independent risk factors. In addition, the level of TIIS significantly influenced drug sensitivity, including sensitivity to Cisplatin. While the hub genes are more highly expressed in normal tissues and often indicate better outcomes, the TIIS, as a predictive scoring system, is associated with an immunosuppressive TME and poor prognosis. This discrepancy may reflect the complex interactions within the TME. Specifically, these hub genes might play dual roles, contributing to immune suppression or promoting tumor aggressiveness under certain conditions. Alternatively, their expression may serve as a marker for a distinct tumor subtype that responds differently to the TME. Further investigation is required to fully elucidate these intricate mechanisms. The potential involvement of CD2 molecules in monocyte-T cell interactions and their potential role in regulating the balance of CD8+ T cell activation has been suggested in the literature [45, 46]. The increased expression of CD2 in our predictive model may serve to suppress T cell activation. CSF1R is crucial in the process of macrophage polarization, and inhibitors targeting CSF1R have been extensively used in cancer immunotherapy to effectively reduce tumor-associated macrophages (TAMs) [47]. It was observed that myeloid cells exhibited high expression levels of CSF1R, which may lead

to a significant enhancement of M2 macrophage infiltration. CCL5 is a secreted chemokine responsible for the infiltration of NK cells, type I dendritic cells, type 1 T helper cells and type 1 cytotoxic cells. Increased expression of CCL5 in tumors can lead to the enhancement of various immune invasions of tumors. Furthermore, CCL5 has been found to be expressed in various cell types within the TME, including CAFs, myeloid-derived suppressor cells, TAMs, and lymphatic endothelial cells, thereby facilitating tumorigenesis and tumor progression [48]. It is hypothesized that in the context of BLCA, CCL5 may be upregulated in CAFs and TAMs, thereby promoting tumor progression. Interferon sequence-binding protein (ICSBP), alternatively referred to as IRF8, serves as a transcription factor belonging to the interferon regulatory factor (IRF) family and exerts a suppressive influence on immune cell function. Specifically, IRF8 is involved in the regulation of dendritic cell autophagy [49]. The increased expression of IRF8 in myeloid cells in our model was likely to enhance dendritic cell apoptosis, thereby increasing the immunosuppressive milieu of the TME. In conclusion, our study established a prognostic model based on the hub genes in TIICs that could also reflect drug response and guide the treatment of BLCA patients. TYROBP, a transmembrane signaling polypeptide with an immunoreceptor tyrosine-based activation motif (ITAM) in its cytoplasmic domain, was shown to be predominantly expressed in myeloid cells in the scRNA-seq dataset. Previous research has shown that increased TYROBP expression serves as an independent prognostic risk factor in glioma. Dysregulation of TYROBP expression was associated with immune infiltration and represented a potential therapeutic target and prognostic indicator for glioma [50]. This was consistent with the results of our model, which suggested that patient prognosis was significantly worse when myeloid cells exhibited high levels of TYROP expression. HLA-DPA1 and HLA-DRA are well recognized for their roles in antigen processing and presentation and are frequently associated with various types of cancer. In the context of colorectal cancer, increased expression of genes involved in antigen presentation has been shown to promote a favorable immune response microenvironment and potentially enhance the efficacy of PD-L1 therapy in BRAF-mutant colorectal tumors [51]. In our model, HLA-DPA1 and HLA-DRA were mainly expressed in BLCA epithelial cells, which may enhance the antigen-presenting capacity of BLCA tumor cells themselves, rather than affecting the function of TIICs, thereby recruiting increasing numbers of T cells in the TME.

This study has several limitations. First, clinically relevant information such as patients' clinical symptoms, examination reports, and medication use for disease treatment was lacking. Second, the study was approached solely from a gene transcriptome perspective and did not include multi-omics verification. Third, the data analysis relied solely on bioinformatics methods, which requires further validation by in vivo and in vitro experiments. Additionally, our analysis did not include datasets with matched pre- and post-treatment samples, limiting our ability to fully capture the dynamic nature of the TME. Moreover, the RNA-seq and scRNA-seq datasets used in our study included BLCA samples from patients at various stages of tumor evolution. While this approach aimed to enhance the model's generalizability, it may have reduced the focus on stage-specific TME characteristics, potentially overlooking the intricate changes associated with tumor progression. Finally, the specific mechanism of immune cell infiltration on drug susceptibility was not thoroughly investigated.

In conclusion, our research established a prognostic scoring system to predict the outcomes of BLCA patients and explored the impact of six hub genes on immune infiltration in BLCA through bioinformatics analysis. Additionally, we identified potential drug candidates that demonstrated sensitivity in specific patient groups, providing new perspectives for the treatment of BLCA.

Acknowledgements Thanks to the public databases for providing us with data, and thanks to the developers of R software and R packages for their contributions and convenience.

Author contributions CL and BSS: data curation, methodology, formal analysis, writing—original draft, writing—review & editing; CL and CYL: data curation, formal analysis, visualization, writing—original draft, writing—review & editing; ZG: data curation, formal analysis, writing—original draft, writing—review & editing; SHC: data curation, methodology, writing—review & editing; SXL: methodology, writing—review & editing; XYY: methodology, writing—review & editing; ZYH: methodology, writing—review & editing; JGL: methodology, writing—review & editing; MD: methodology, writing—review & editing; KW: methodology, writing—review & editing; RXW: conceptualization, methodology supervision, writing—original draft, writing—review & editing; CL and JZ: conceptualization, funding acquisition, supervision, writing—original draft, writing—review & editing; XYD: conceptualization, funding acquisition, supervision, writing—original draft, writing—review & editing.

Funding This study was supported by the Key Project of Chongqing Natural Science Foundation (CSTB2023NSCQ-ZDJ0013), the General Project of Chongqing Natural Science Foundation (2022NSCQ-MSX5657), the Key Project of Young Doctor Incubation Program of the Second Affiliated Hospital of Army Medical University (2023YQB018) and the Central University Basic Research Business Fee Special Project (2022CDJYGRH-020).

Data availability The datasets presented in this study can be found in online repositories. The names of the repository/repositories and accession number(s) can be found in the article.

Declarations

Conflict of interest The authors declare that the research was conducted in the absence of any commercial or financial relationships that could be construed as a potential conflict of interest. The authors declare no competing interests.

Ethical approval Because the datasets used in this study are accessible to the general public, ethical approval was not necessary.

Consent for publication All authors approved the submitted version.

References

1. Lobo N, Afferi L, Moschini M, Mostafid H, Porten S, Psutka SP, Gupta S, Smith AB, Williams SB, Lotan Y. Epidemiology, screening, and prevention of bladder cancer. Eur Urol Oncol. 2022;5:628–39.
2. Kamat AM, Hahn NM, Efstathiou JA, Lerner SP, Malmström PU, Choi W, Guo CC, Lotan Y, Kassouf W. Bladder cancer. Lancet (London, England). 2016;388:2796–810.
3. Xia C, Dong X, Li H, Cao M, Sun D, He S, Yang F, Yan X, Zhang S, Li N, Chen W. Cancer statistics in China and United States, 2022: profiles, trends, and determinants. Chin Med J. 2022;135:584–90.
4. Powles T, Bellmunt J, Comperat E, De Santis M, Huddart R, Loriot Y, Necchi A, Valderrama BP, Ravaud A, Shariat SF, Szabados B, van der Heijden MS, Gillessen S. Bladder cancer: ESMO clinical practice guideline for diagnosis, treatment and follow-up. Ann Oncol. 2022;33:244–58.
5. Liu J, Gao Y, Song C, Liao W, Meng L, Yang S, Xiong Y. Immunotherapeutic prospects and progress in bladder cancer. J Cell Mol Med. 2024;28:e18101.
6. Bedard PL, Hansen AR, Ratain MJ, Siu LL. Tumour heterogeneity in the clinic. Nature. 2013;501:355–64.
7. de Visser KE, Joyce JA. The evolving tumor microenvironment: from cancer initiation to metastatic outgrowth. Cancer Cell. 2023;41:374–403.
8. Dyugay IA, Lukyanov DK, Turchaninova MA, Serebrovskaya EO, Bryushkova EA, Zaretsky AR, Khalmurzaev O, Matveev VB, Shugay M, Shelyakin PV, Chudakov DM. Accounting for B-cell behavior and sampling bias predicts anti-PD-L1 response in bladder cancer. Cancer Immunol Res. 2022;10:343–53.
9. Oh DY, Kwek SS, Raju SS, Li T, McCarthy E, Chow E, Aran D, Ilano A, Pai CS, Rancan C, Allaire K, Burra A, Sun Y, Spitzer MH, Mangul S, Porten S, Meng MV, Friedlander TW, Ye CJ, Fong L. Intratumoral CD4(+) T cells mediate anti-tumor cytotoxicity in human bladder cancer. Cell. 2020;181:1612-1625.e13.
10. Chen Z, Zhou L, Liu L, Hou Y, Xiong M, Yang Y, Hu J, Chen K. Single-cell RNA sequencing highlights the role of inflammatory cancer-associated fibroblasts in bladder urothelial carcinoma. Nat Commun. 2020;11:5077.
11. Wang F, Zhang G, Xu T, Ma J, Wang J, Liu S, Tang Y, Jin S, Li J, Xing N. High and selective cytotoxicity of ex vivo expanded allogeneic human natural killer cells from peripheral blood against bladder cancer: implications for natural killer cell instillation after transurethral resection of bladder tumor. J Exp Clin Cancer Res. 2024;43:24.
12. Goulet CR, Champagne A, Bernard G, Vandal D, Chabaud S, Pouliot F, Bolduc S. Cancer-associated fibroblasts induce epithelial-mesenchymal transition of bladder cancer cells through paracrine IL-6 signalling. BMC Cancer. 2019;19:137.
13. Qiu L, Liu X. Identification of key genes involved in myocardial infarction. Eur J Med Res. 2019;24:22.
14. Zhao X, Zhang L, Wang J, Zhang M, Song Z, Ni B, You Y. Correction to: Identification of key biomarkers and immune infiltration in systemic lupus erythematosus by integrated bioinformatics analysis. J Transl Med. 2021;19:64.
15. Burr ML, Sparbier CE, Chan KL, Chan YC, Kersbergen A, Lam EYN, Azidis-Yates E, Vassiliadis D, Bell CC, Gilan O, Jackson S, Tan L, Wong SQ, Hollizeck S, Michalak EM, Siddle HV, McCabe MT, Prinjha RK, Guerra GR, Solomon BJ, Sandhu S, Dawson SJ, Beavis PA, Tothill RW, Cullinane C, Lehner PJ, Sutherland KD, Dawson MA. An evolutionarily conserved function of polycomb silences the MHC class I antigen presentation pathway and enables immune evasion in cancer. Cancer Cell. 2019;36:385-401.e8.
16. Chung W, Eum HH, Lee HO, Lee KM, Lee HB, Kim KT, Ryu HS, Kim S, Lee JE, Park YH, Kan Z, Han W, Park WY. Single-cell RNA-seq enables comprehensive tumour and immune cell profiling in primary breast cancer. Nat Commun. 2017;8:15081.
17. Chawla S, Rockstroh A, Lehman M, Ratther E, Jain A, Anand A, Gupta A, Bhattacharya N, Poonia S, Rai P, Das N, Majumdar A, Jayadeva, Ahuja G, Hollier BG, Nelson CC, Sengupta D. Gene expression based inference of cancer drug sensitivity. Nat Commun. 2022;13:5680.
18. Kim WJ, Kim EJ, Kim SK, Kim YJ, Ha YS, Jeong P, Kim MJ, Yun SJ, Lee KM, Moon SK, Lee SC, Cha EJ, Bae SC. Predictive value of progression-related gene classifier in primary non-muscle invasive bladder cancer. Mol Cancer. 2010;9:3.
19. Lee JS, Leem SH, Lee SY, Kim SC, Park ES, Kim SB, Kim SK, Kim YJ, Kim WJ, Chu IS. Expression signature of E2F1 and its associated genes predict superficial to invasive progression of bladder tumors. J Clin Oncol. 2010;28:2660–7.
20. Mariathasan S, Turley SJ, Nickles D, Castiglioni A, Yuen K, Wang Y, Kadel EE III, Koeppen H, Astarita JL, Cubas R, Jhunjhunwala S, Banchereau R, Yang Y, Guan Y, Chalouni C, Ziai J, Şenbabaoğlu Y, Santoro S, Sheinson D, Hung J, Giltnane JM, Pierce AA, Mesh K, Lianoglou S, Riegler J, Carano RAD, Eriksson P, Höglund M, Somarriba L, Halligan DL, van der Heijden MS, Loriot Y, Rosenberg JE, Fong L, Mellman I, Chen DS,

Green M, Derleth C, Fine GD, Hegde PS, Bourgon R, Powles T. TGFβ attenuates tumour response to PD-L1 blockade by contributing to exclusion of T cells. Nature. 2018;554:544–8.
21. Choi W, Porten S, Kim S, Willis D, Plimack ER, Hoffman-Censits J, Roth B, Cheng T, Tran M, Lee IL, Melquist J, Bondaruk J, Majewski T, Zhang S, Pretzsch S, Baggerly K, Siefker-Radtke A, Czerniak B, Dinney CP, McConkey DJ. Identification of distinct basal and luminal subtypes of muscle-invasive bladder cancer with different sensitivities to frontline chemotherapy. Cancer Cell. 2014;25:152–65.
22. Guo CC, Bondaruk J, Yao H, Wang Z, Zhang L, Lee S, Lee JG, Cogdell D, Zhang M, Yang G, Dadhania V, Choi W, Wei P, Gao J, Theodorescu D, Logothetis C, Dinney C, Kimmel M, Weinstein JN, McConkey DJ, Czerniak B. Assessment of luminal and basal phenotypes in bladder cancer. Sci Rep. 2020;10:9743.
23. Gouin KH 3rd, Ing N, Plummer JT, Rosser CJ, Ben Cheikh B, Oh C, Chen SS, Chan KS, Furuya H, Tourtellotte WG, Knott SRV, Theodorescu D. An N-Cadherin 2 expressing epithelial cell subpopulation predicts response to surgery, chemotherapy and immunotherapy in bladder cancer. Nat Commun. 2021;12:4906.
24. Zeng D, Ye Z, Shen R, Yu G, Wu J, Xiong Y, Zhou R, Qiu W, Huang N, Sun L, Li X, Bin J, Liao Y, Shi M, Liao W. IOBR: multi-omics immuno-oncology biological research to decode tumor microenvironment and signatures. Front Immunol. 2021;12:687975.
25. Hao Y, Stuart T, Kowalski MH, Choudhary S, Hoffman P, Hartman A, Srivastava A, Molla G, Madad S, Fernandez-Granda C, Satija R. Dictionary learning for integrative, multimodal and scalable single-cell analysis. Nat Biotechnol. 2024;42:293–304.
26. Ritchie ME, Phipson B, Wu D, Hu Y, Law CW, Shi W, Smyth GK. limma powers differential expression analyses for RNA-sequencing and microarray studies. Nucleic Acids Res. 2015;43:e47.
27. Zhang Y, He R, Lei X, Mao L, Jiang P, Ni C, Yin Z, Zhong X, Chen C, Zheng Q, Li D. A novel pyroptosis-related signature for predicting prognosis and indicating immune microenvironment features in osteosarcoma. Front Genet. 2021;12:780780.
28. Langfelder P, Horvath S. WGCNA: an R package for weighted correlation network analysis. BMC Bioinform. 2008;9:559.
29. Szklarczyk D, Gable AL, Lyon D, Junge A, Wyder S, Huerta-Cepas J, Simonovic M, Doncheva NT, Morris JH, Bork P, Jensen LJ, Mering CV. STRING v11: protein-protein association networks with increased coverage, supporting functional discovery in genome-wide experimental datasets. Nucleic Acids Res. 2019;47:D607-d613.
30. Shannon P, Markiel A, Ozier O, Baliga NS, Wang JT, Ramage D, Amin N, Schwikowski B, Ideker T. Cytoscape: a software environment for integrated models of biomolecular interaction networks. Genome Res. 2003;13:2498–504.
31. Zhou Y, Zhou B, Pache L, Chang M, Khodabakhshi AH, Tanaseichuk O, Benner C, Chanda SK. Metascape provides a biologist-oriented resource for the analysis of systems-level datasets. Nat Commun. 2019;10:1523.
32. Tang Z, Kang B, Li C, Chen T, Zhang Z. GEPIA2: an enhanced web server for large-scale expression profiling and interactive analysis. Nucleic Acids Res. 2019;47:W556-w560.
33. Yosefian I, Farkhani EM, Baneshi MR. Application of random forest survival models to increase generalizability of decision trees: a case study in acute myocardial infarction. Comput Math Methods Med. 2015;2015:576413.
34. Wang X, Gong G, Li N, Qiu S. Detection analysis of epileptic EEG using a novel random forest model combined with grid search optimization. Front Hum Neurosci. 2019;13:52.
35. Newman AM, Liu CL, Green MR, Gentles AJ, Feng W, Xu Y, Hoang CD, Diehn M, Alizadeh AA. Robust enumeration of cell subsets from tissue expression profiles. Nat Methods. 2015;12:453–7.
36. Yoshihara K, Shahmoradgoli M, Martínez E, Vegesna R, Kim H, Torres-Garcia W, Treviño V, Shen H, Laird PW, Levine DA, Carter SL, Getz G, Stemke-Hale K, Mills GB, Verhaak RG. Inferring tumour purity and stromal and immune cell admixture from expression data. Nat Commun. 2013;4:2612.
37. Finotello F, Mayer C, Plattner C, Laschober G, Rieder D, Hackl H, Krogsdam A, Loncova Z, Posch W, Wilflingseder D, Sopper S, Ijsselsteijn M, Brouwer TP, Johnson D, Xu Y, Wang Y, Sanders ME, Estrada MV, Ericsson-Gonzalez P, Charoentong P, Balko J, de Miranda N, Trajanoski Z. Molecular and pharmacological modulators of the tumor immune contexture revealed by deconvolution of RNA-seq data. Genome Med. 2019;11:34.
38. Li B, Severson E, Pignon JC, Zhao H, Li T, Novak J, Jiang P, Shen H, Aster JC, Rodig S, Signoretti S, Liu JS, Liu XS. Comprehensive analyses of tumor immunity: implications for cancer immunotherapy. Genome Biol. 2016;17:174.
39. Charoentong P, Finotello F, Angelova M, Mayer C, Efremova M, Rieder D, Hackl H, Trajanoski Z. Pan-cancer immunogenomic analyses reveal genotype-immunophenotype relationships and predictors of response to checkpoint blockade. Cell Rep. 2017;18:248–62.
40. Racle J, de Jonge K, Baumgaertner P, Speiser DE, Gfeller D. Simultaneous enumeration of cancer and immune cell types from bulk tumor gene expression data. Elife. 2017;6:e26476.
41. Hänzelmann S, Castelo R, Guinney J. GSVA: gene set variation analysis for microarray and RNA-seq data. BMC Bioinform. 2013;14:7.
42. Maeser D, Gruener RF, Huang RS. oncoPredict: an R package for predicting in vivo or cancer patient drug response and biomarkers from cell line screening data. Brief Bioinform. 2021. https://doi.org/10.1093/bib/bbab260.
43. Liao C, Wang X. TCGAplot: an R package for integrative pan-cancer analysis and visualization of TCGA multi-omics data. BMC Bioinform. 2023;24:483.
44. Robertson AG, Kim J, Al-Ahmadie H, Bellmunt J, Guo G, Cherniack AD, Hinoue T, Laird PW, Hoadley KA, Akbani R, Castro MAA, Gibb EA, Kanchi RS, Gordenin DA, Shukla SA, Sanchez-Vega F, Hansel DE, Czerniak BA, Reuter VE, Su X, de Sa Carvalho B, Chagas VS, Mungall KL, Sadeghi S, Pedamallu CS, Lu Y, Klimczak LJ, Zhang J, Choo C, Ojesina AI, Bullman S, Leraas KM, Lichtenberg TM, Wu CJ, Schultz N, Getz G, Meyerson M, Mills GB, McConkey DJ, Weinstein JN, Kwiatkowski DJ, Lerner SP. Comprehensive molecular characterization of muscle-invasive bladder cancer. Cell. 2017;171:540-556.e25.
45. Abplanalp WT, Cremer S, John D, Hoffmann J, Schuhmacher B, Merten M, Rieger MA, Vasa-Nicotera M, Zeiher AM, Dimmeler S. Clonal hematopoiesis-driver DNMT3A mutations alter immune cells in heart failure. Circ Res. 2021;128:216–28.
46. McKinney EF, Lee JC, Jayne DR, Lyons PA, Smith KG. T-cell exhaustion, co-stimulation and clinical outcome in autoimmunity and infection. Nature. 2015;523:612–6.
47. Banuelos A, Zhang A, Berouti H, Baez M, Yılmaz L, Georgeos N, Marjon KD, Miyanishi M, Weissman IL. CXCR2 inhibition in G-MDSCs enhances CD47 blockade for melanoma tumor cell clearance. Proc Natl Acad Sci USA. 2024;121:e2318534121.
48. Korbecki J, Grochans S, Gutowska I, Barczak K, Baranowska-Bosiacka I. CC chemokines in a tumor: a review of pro-cancer and anti-cancer properties of receptors CCR5, CCR6, CCR7, CCR8, CCR9, and CCR10 ligands. Int J Mol Sci. 2020;21:7619.

49. Agod Z, Pazmandi K, Bencze D, Vereb G, Biro T, Szabo A, Rajnavolgyi E, Bacsi A, Engel P, Lanyi A. Signaling lymphocyte activation molecule family 5 enhances autophagy and fine-tunes cytokine response in monocyte-derived dendritic cells via stabilization of interferon regulatory factor 8. Front Immunol. 2018;9:62.
50. Lu J, Peng Y, Huang R, Feng Z, Fan Y, Wang H, Zeng Z, Ji Y, Wang Y, Wang Z. Elevated TYROBP expression predicts poor prognosis and high tumor immune infiltration in patients with low-grade glioma. BMC Cancer. 2021;21:723.
51. Morafraile EC, Saiz-Ladera C, Nieto-Jiménez C, Győrffy B, Nagy A, Velasco G, Pérez-Segura P, Ocaña A. Mapping immune correlates and surfaceome genes in BRAF mutated colorectal cancers. Curr Oncol (Toronto, Ont). 2023;30:2569–81.